J. Hydrol. Hydromech., 71, 2023, 4, 369–381
https://doi.org/10.2478/johh-2023-0034
© Milan Gomboš et al., published by Sciendo. This work is licensed under the Creative Commons Attribution-NonCommercial-NoDerivatives 4.0 International Licence.

sciendo Journal of Hydrology and Hydromechanics Institute of Hydrology SAS

Changes in crack width on the surface of heavy soils during drought, determined by precise measurement and calculation

Milan Gomboš[1], Andrej Tall[1], Branislav Kandra[1], Anca Constantin[2], Dana Pavelkova[1*]

[1] Institute of Hydrology, Slovak Academy of Sciences, Dúbravská cesta 9, 841 04 Bratislava, Slovakia.
[2] Ovidius University from Constanta, Faculty of Civil Engineering, 22b Unirii str, Constanta, Romania.
[*] Corresponding author. E-mail: pavelkova@uh.savba.sk

Abstract: In heavy soils, changes in humidity incur soil volume changes. In the horizontal plane, these are manifested by cracks formation and in the vertical plane by the movement of the soil surface. Cracks have a significant impact on hydrodynamics of the soil profile. The work is based on the hypothesis that soil volume changes depend on both the content of clay particles in soil and soil volumetric moisture. The aim of the work is to measure and analyze the changes in the width of the cracks and their reaction to the changes in volumetric soil moisture. One of the objectives of the work was to design a simple tool for accurate measurement and calculation of the crack width on the soil surface. For the study of crack width, a soil profile in an area on the East Slovakia Lowland was selected. The profile was examined under conditions of extreme drought, at the turn of July and August 2022. Crack width varied between 1.0 cm and 3.3 cm. The calculation procedure was evaluated as satisfactory for estimating the change in crack width on the soil surface.

Keywords: Heavy soil; Crack width; Volume changes; Volumetric soil moisture.

INTRODUCTION

Cracks on the soil surface are the gateway for water to the unsaturated zone at its upper boundary.

In heavy soils, high content of clay minerals can lead to their volume changes when soil moisture changes. The crystals of some clay minerals have the ability to bind variable water content in their structure (Johnston, 2018; Velde, 1995). As the water content increases, clay swells, but it regains its original volume when dried (Amorim et al., 2007; Chen et al., 2022; Crescimanno et al., 1995; Čurlík and Bedrna, 1971; Hansen et al. 2012; Ross, 1978). Volume changes are a three-dimensional process. In the horizontal plane, the changes are manifested by formation of cracks and in the vertical plane by vertical movement of the soil surface. Consisting of a cracks domain and a soil matrix domain, a two-domain soil structure is created when cracks are formed (Beven and Germann, 1982; Gerke and van Genuchten, 1993; Jarvis, 1994; Tang et al., 2023). Spatially, shrinkage cracks are scattered within the unsaturated zone of a soil profile. The above-mentioned facts indicate that the content of clay minerals in soils affects their hydro-physical properties. Crystal and chemical structure of clay minerals reacts very sensitively to hydrothermal environment and its physical and chemical properties. The content of clay minerals is specific for each soil type. It is one of the soil type characteristics features. In contrast, soil moisture changes by hydro-meteorological conditions in the area, the depth of the unsaturated soil zone and anthropogenic activity (Almikaeel et al., 2022; Baroková et al., 2020; Čubanová et al., 2022; Đukić et al., 2021; Kuban et al., 2022) in the area. This is reflected in the dynamics of hydrological processes. In light soils with a lower content of clay particles, i.e. with no crack formation, the movement of water in the unsaturated zone is well explored. It is described by the Richards equation (Richards, 1931). The equation is based on the assumption of laminar flow in small pores. Several mathematical simulation models have been created to describe the water flow in the pore environment of rigid soils, which provide numerical solution of water movement in the unsaturated soil zone (Benetin et al., 1985; Ross, 1990; Šimůnek et al., 2017; Zurmuhl and Durner, 1996). The situation becomes more complicated with the increased clay content in soils. In clay and clay-loamy soils (also called heavy soils) with a high proportion of clay minerals mainly of the illitic and montmorillonite groups, the water movement resembles the movement in rigid soils, but only until the first cracks are formed. The presence of shrinkage cracks significantly changes the hydrodynamic properties of a soil profile. This makes it impossible to use the methods that work successfully for describing the hydrological processes in rigid soils. The soil profile of heavy soils containing shrinkage cracks forms a two-component system consisting of cracks (also called macropores) and the soil matrix (which includes micropores). Each of these components creates very different conditions for water transfer and retention (Bronswijk, 1988; 1990; Bronswijk and Evers-Vermeer, 1990; Doležal, 2001; Hallett et al., 2013; van Genuchten et al., 2000). When a large amount of water enters the soil in a short time and the cracks have not closed yet, rainwater movement in the cracks is analogous to water movement in an open ditch. Rate of water movement is higher by orders of magnitude in comparison with water movement through micropores. The crack network forms a system of preferred water flow paths in both horizontal (horizontal conductivity of cracks) and vertical (vertical conductivity of cracks) direction. Cracks geometry changes in time and therefore hydraulic parameters of the preferred paths change as well (Chertkov, 2001; 2002; Chertkov and Ravina, 1999; 2011; Stewart and Najm, 2020). Open water level in cracks can exist only if they are still open. The water in cracks rapidly increases soil moisture and thus accelerates the cracks closure. This indicates that the water movement in cracks is limited by the soil response time to moisture changes. In the study of a two-domain soil structure, unlike in the study of rigid soils, it is necessary to consider and quantify the phenomena caused by soil volumetric

changes, such as definition of crack network geometry, soil surface vertical movement, shrinkage characteristics, shrinkage potential, water flow to cracks, water flow within cracks and water flow from cracks to soil matrix (Krisnanto et al., 2016; Novák, 1978; 2000; Novák and Šoltész, 1994). These processes and their characteristics are unique and site-specific in their nature, which means that the application of experimental studies to different locations is debatable.

In the East-Slovakian Lowland (ESL), the cracks are larger and appear earlier in season compared to the past. This is due to the duration of rainless periods and warmer springs. Despite relatively high level of groundwater on ESL, the formation of cracks in soils with a lower content of clay particles has been observed more frequently in recent years. Capillary inflow from groundwater to a soil profile was insufficient for mitigating this phenomenon. From this point of view, cracks formation signals soil drought. On the other side of the extreme conditions are sudden and extreme precipitation events during a dry season. The crack network with its retention volume affects the rainfall-runoff and other water transport processes in the area.

It is necessary to deepen our knowledge on water regime management and the dynamics of soil water supply in heavy soils in order to forecast their future development. This requires sound knowledge on the hydrological processes in natural environment and on the elements that influence these processes.

The aim of the work is (a) to monitor in field and subsequently analyze the cracks width and dynamics of cracks width changes in the surface soil layer 0.0–0.1 m; (b) to monitor dynamics of cracks width changes at sudden precipitation event; (c) to measure air temperature in the crack 0.1 m under the soil surface, on the soil surface and 2 m above the soil surface in order to illustrate temperature conditions (Tang et al., 2010); (d) based on the measured hydro-physical parameters and volumetric moisture of the soil to suggest calculation method for determining cracks width on the unit surface area; (e) to verify calculated values against measured values.

METHODOLOGY

Site description

The investigated site of Milhostov is situated in the central part of the ESL (Fig. 1). The ESL with an area 2 638 km^2 represents the northernmost part of the extensive Inner Carpathians tectonic depression. It was formed by uneven tectonic subsidence of the Earth crust within the Carpathian arc in the Neogene and Quaternary. Soil conditions correspond to geological conditions. ESL is characterized by a high proportion of heavy and very heavy soils (Table 1). Climate-wise, the area of ESL lies in the transition zone between oceanic and continental climate. The area belongs to a warm, slightly humid region with cold winters. The climate, and thus all meteorological elements, is greatly variable. This is reflected in rapid change of air masses in every season and general cyclonic activity. Characteristic feature of the area is mainly the degree of continentality. In terms of temperature, ESL is a homogenous area. The long-term average temperature in this region is around 9.6 °C. The coldest month of the year during the investigated period was January (–2.8 °C) and the warmest was July (20.5 °C). Circulation factors are decisive for the formation of precipitation. On ESL, precipitation occurs mainly when the area is hit by humid and warm air currents from the south. Air masses bearing precipitation which come from the west, north and east are depleted of the precipitation that fall on the slopes of the Carpathian mountain range. This is reflected in the spatial distribution of rainfall. The area with minimum annual precipitation total (below 600 mm) is located in the central and southwest part of the lowland. Towards the west and northeast, the volume of precipitation increases, with annual precipitation totals between 800 mm and 900 mm.

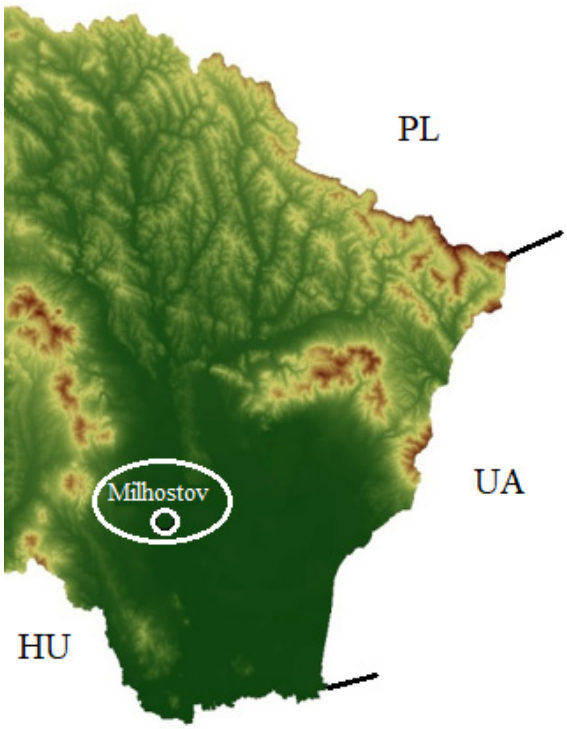


Fig. 1. Location of the investigated area.

Table 1. The proportion of soil types in the East-Slovakian Lowland.

soil types				
light soils	medium heavy soils		heavy soils	very heavy soils
sand loamy sand	sandy loam	loam	clay loam	clay
[%]	[%]	[%]	[%]	[%]
2.6	50.7	4.9	21.9	19.9

For the study of the cracks width, a soil profile in Milhostov area (48° 40.183´N; 21° 44.300´E) was selected (Fig. 1). The area is covered with silt-clay loams, (Fig. 2a) which alter into sandy loam in the deeper soil horizons (80 cm) (Fig. 2b). The cracks width in the selected profile was studied in the upper layer of the soil horizon, 0.0–0.1 m. The greatest changes in volumetric moisture and thus soil volume changes are assumed to occur in this layer. Soil microstructure in this layer consists of 33.3% of clay (soil particles ≤ 0.002 mm), 58.4% of silt (0.002 mm, 0.05 mm⟩, 8.3% of sand (0.05 mm, 2.0 mm⟩. The average retention characteristics of the investigated soil profile to depths of 1 m, expressed by hydrolimits (notable thresholds on the retention curve), field water capacity (FC), threshold point (TP) and wilting point (WP), are shown in Table 2.

Table 2. Retention characteristics of the soil profile to the depth of 1 m.

Locality	Hydrolimits [%]		
	WP	TP	FC
Milhostov	23	31	42

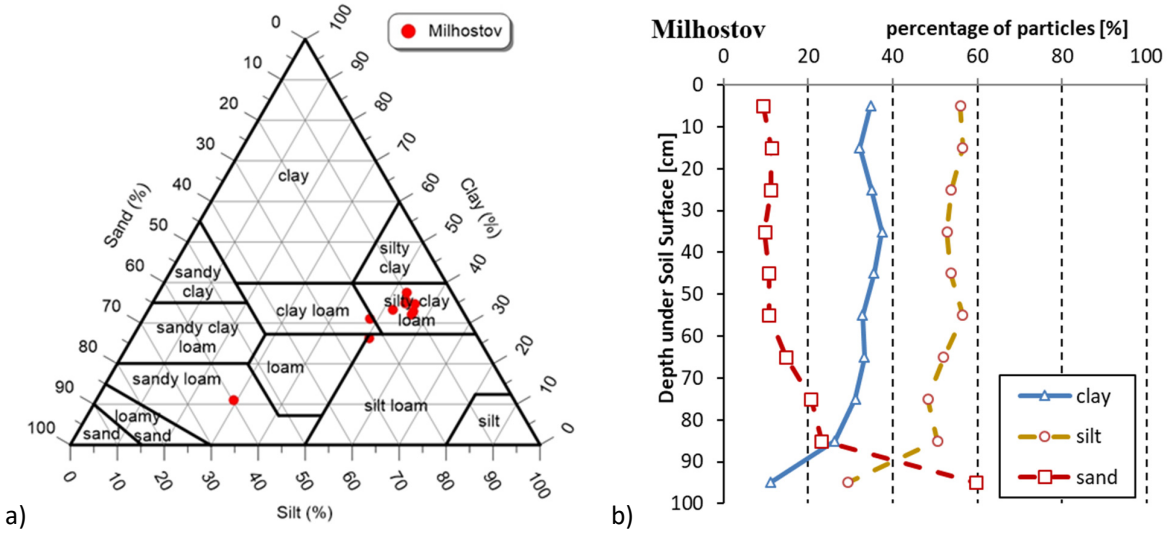


Fig. 2. Identification of soil types (a) and the course of soil texture along the depth of investigated soil profile (b).

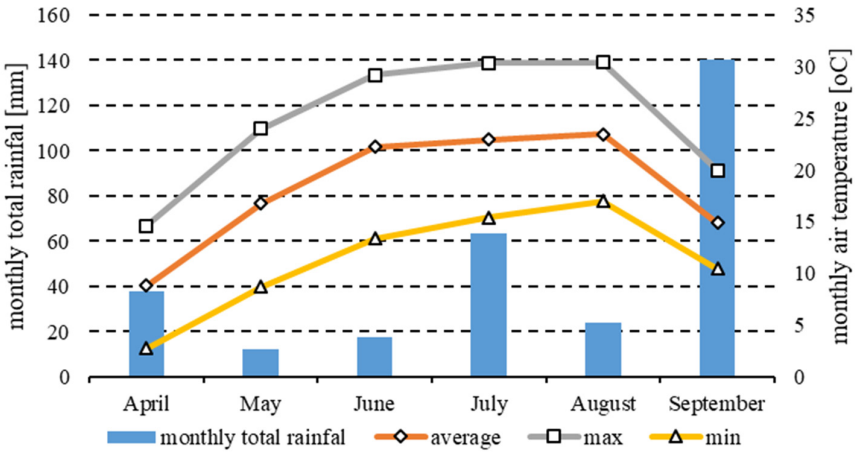


Fig. 3. Average monthly temperatures, maximum and minimum average monthly temperatures and monthly precipitation totals in the growing season of 2022 in Milhostov area.

The hydrolimits in Table 2 were determined from the retention curve for the potential pF 4.2; 3.3; 2.5. Three intact soil samples were taken in a layer 30–40 cm under the soil surface. The measurement of the moisture potential was realized by pressure plate method (Dane and Hopmans, 2002). Measured pressure values were selected for the retention curve according to ISO 11274 (Cools and De Vos, 2010; ISO 11274, 1998). For the sake of simplicity, the identified retention curve was considered for the entire investigated profile.

In the investigated area, regular monitoring of volumetric moisture is carried out to the depth of 1 m by 0.1 m thick layers during the growing season. Volumetric moisture is determined by the gravimetric method. The growing season of 2022 was selected for the presentation of the monitoring results. In this growing season (April–September), the precipitation total in Milhostov was 295.4 mm, which represents 13% probability of occurrence in the 53-year series of measurements. In this context, it should be noted that 47.5% (140.2 mm) of the precipitation total fell at the end of the growing season, i.e. in September (Fig. 3). This had an impact on soil water supplies. Therefore, the growing season of 2022 ranked in the absolute driest periods from 1970.

A very effective method for displaying monitored parameters are contour lines (isolines, isopleths). Contour lines along which the value of soil moisture in a soil profile is the same at different time points are called chronoisopleths. Chronoisopleth helps us make an idea of the temporal development of soil moisture.

Fig. 4 shows the course of volumetric moisture in the investigated soil profile during the growing season of 2022 in the form of chronoisopleths. In Fig. 4, the individual moisture levels are distinguished by colour. It is clear that the entire profile to the depth of 1 m was dried. Drying of the soil profile to the depth of 10 cm started already at the beginning of May. Soil moisture values were continuously below the stress point until mid-September. In some parts of the soil profile, soil moisture decreased below the wilting point (WP). On the ground, grass was dry, which corresponded to the state of soil moisture within the soil profile. Rainfall in September gradually saturated the upper soil horizons until reaching the optimum state.

The stated results are more obvious in Fig. 5. In this figure, the intervals of moisture isolines are represented by hydrolimits FC, TP and WP.

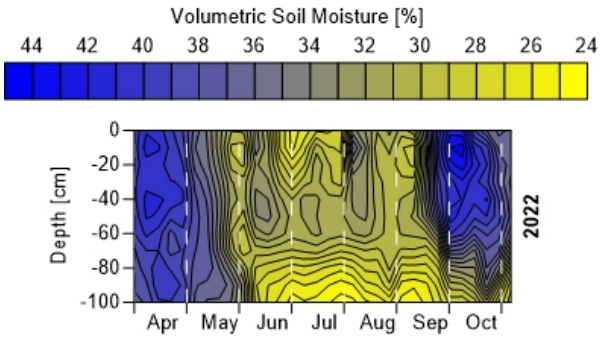


Fig. 4. Contour line of soil moisture course in the investigated soil profile (chronoisopleths), Milhostov area.

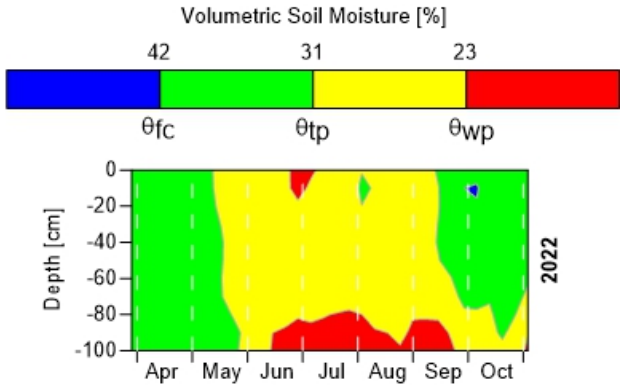


Fig. 5. Contour lines defined by hydrolimits, Milhostov area.

Measurements and calculation

As a result of drought, a two-domain soil structure was formed. The cracks were most noticeable in July. For this reason, from 13.7.2022 to 11.8.2022, measurements of the cracks width were performed at three points (Fig. 6). Points 1, 2 and 3, where cracks width was measured, form the vertices of a triangle. The time domain reflectometry (TDR) sensor TRIME-EZ (IMKO Micromodultechnik GmbH, Germany) was used for the non-destructive measurement of volumetric moisture in the center of gravity of the triangle. Soil volumetric moisture was measured in the upper layer of the soil to a depth of 10 cm, air temperature on the surface and in a crack at a depth of 10 cm under the ground. The daily precipitation totals, maximum and minimum daily air temperature were provided by the meteorological station located in Milhostov area. The meteorological station (48° 39' 47.20" N; 21° 43´17.80" E) and the experimental area (48° 40' 19.64" N; 21° 44' 19.46" E) are located in the center of ESL. Their direct distance is 1610 m. The meteorological station is situated at an altitude of 103 m a.s.l. The experimental area is located at an altitude of 100 m a.s.l. There is no natural or man-made object in their vicinity that would disrupt the homogeneity of hydrometeorological elements in the area where the said objects are located. For that reason, we do not expect statistically significant differences between the meteorological elements at the mentioned points. Basic hydro-physical characteristics were determined in the soil profile. Based on these measurements, the influence of precipitation on the change in crack width on the soil surface was investigated. The measurements were compared with the values calculated from the hydro-physical characteristics.

For measuring the width of cracks, standard devices are used, the common advantage of which is automatic operation. Their review is presented in studies (Stewart and Najm, 2020; Tang et al., 2021). None of these devices were available at our workplace. For this reason, simple but effective tool was designed to accurately measure the width of cracks on the soil surface. It consists of two hinged arms (Fig. 7). The hinged arms move along a rail placed on the surface of the ground. This ensures a stable vertical position of the arms in the crack. A flexible bag filled with water is placed above the rail. Its task is to ensure constant contact of the hinged arms with the walls of the crack at ground level when the geometric dimensions of the crack change. The wall of the bag consists of two 0.55 mm thick rubber layers. Volume of the bag is 150 cm^3. The outer spread on the upper edge of the arms of the tool is measured.

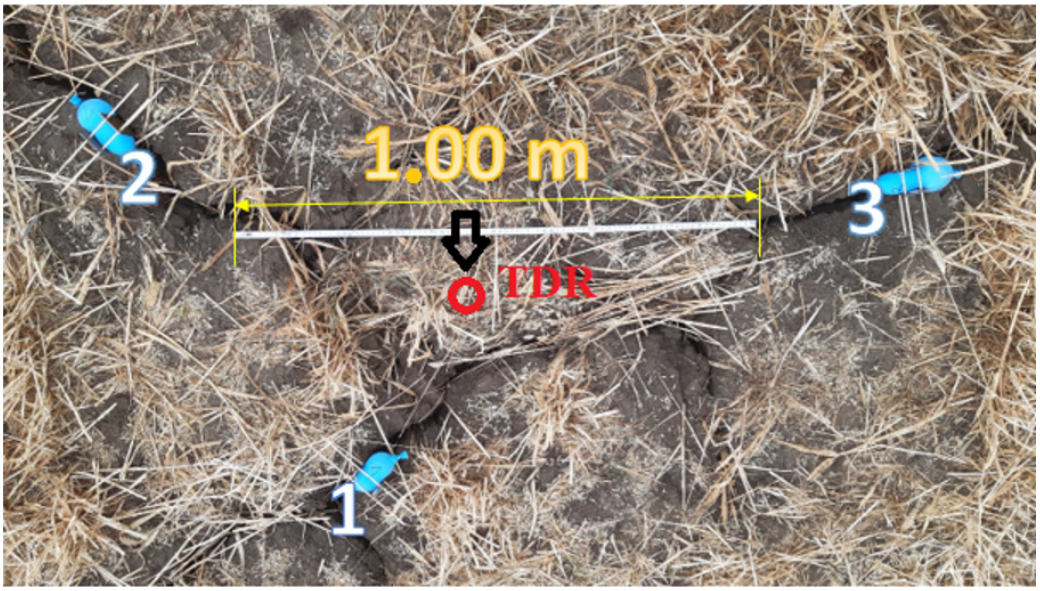


Fig. 6. Measuring the width of cracks on the surface of the soil profile.

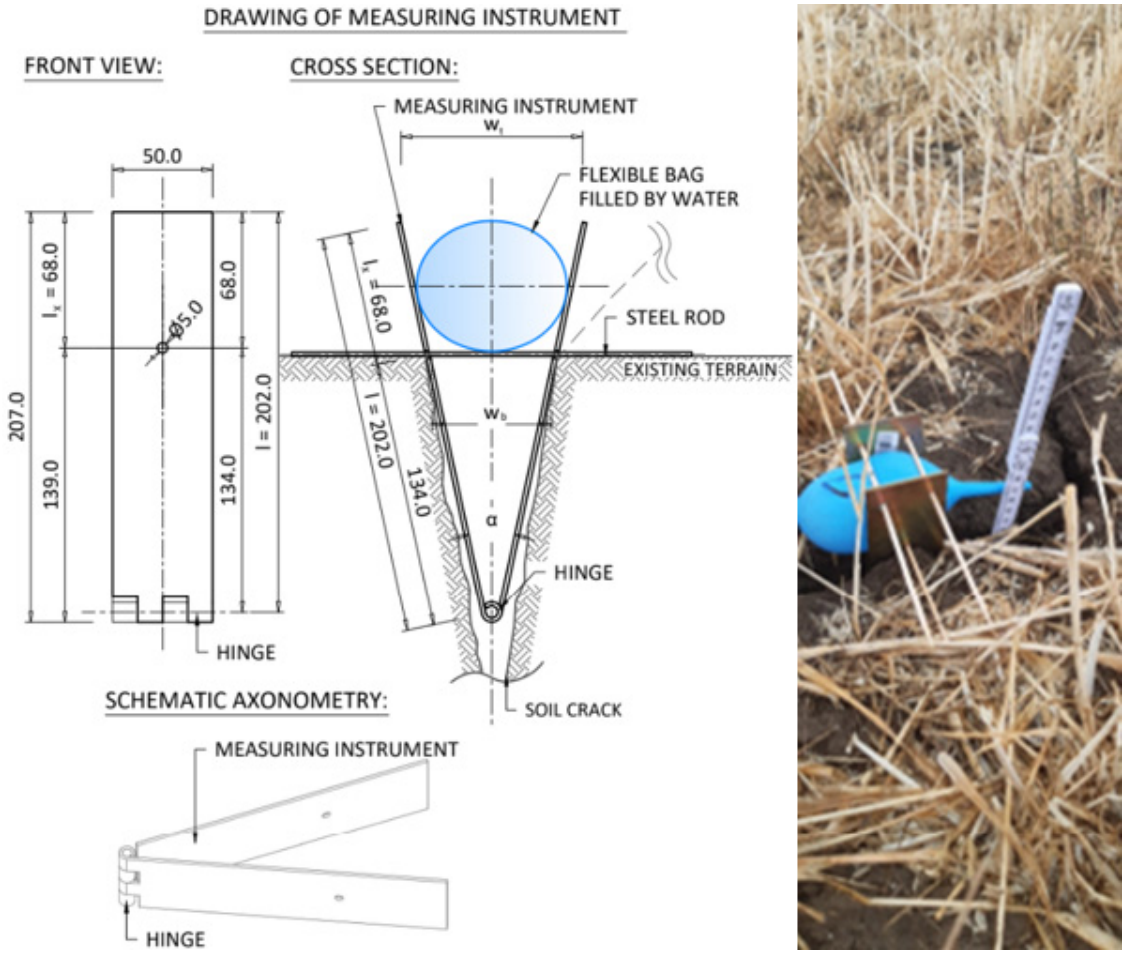


Fig. 7. Scheme of the tool for measuring the width of cracks on the soil surface and its installation in the field.

Due to different heights of the tool installation in the crack, there is a different degree of precision in measuring the crack width. To calculate the actual crack width on the soil surface from the measured data, the following terms apply:

$$\frac{w_t}{w_b} = \frac{l}{l - l_x} \tag{1}$$

$$w_b = \frac{l - l_x}{l} w_t = k\, w_t \tag{2}$$

$$en = \frac{1}{k} \tag{3}$$

where l is the total length of the hinged arm of the measuring tool; l_x is the length of the arm of the measuring tool above the crack surface; w_t is the external expansion on the upper edge of the hinged arms of the measuring tool; w_b is the width of the crack on the soil surface, k is the conversion constant of the tool; en is the rate of increase in the crack measurement.

The tool can be effectively used if the condition below applies:

$$2(l - l_x) \gg w_b \tag{4}$$

The formation of cracks in soil is a manifestation of volume changes. For the calculation, it is necessary to identify the isotropy of the processes participating in the volume changes. If the shrinkage is not isotropic, it is necessary to quantify the part of the volume changes that is transformed into the crack network volume and the part which is transformed into the vertical movement of soil surface (Bronswijk, 1988; 1990). These relations can be derived based on the simple reasoning. A saturated cube-shaped soil sample with edge z_s has a volume of $V_s = z_s^3$. After isotropic shrinkage, the saturated sample is reduced by volume V_r to a cube with edge $z = z_s - \Delta z$ and volume $V = z^3$.

Based on the above, it is possible to formulate a relationship:

$$\frac{V}{V_s} = \frac{V_s - V_r}{V_s} = \frac{z^3}{z_s^3} = \frac{(z_s - \Delta z)^3}{z_s^3} \tag{5}$$

On the basis of Equation (5) it is possible to deduce the relationships for calculating the geometric factor for assessing the isotropy of volume changes and the relationship between the change in volume and height (between volume changes in both vertical and horizontal direction). If the parameters are V, V_s, Δz, z_s, are measured then the geometric factor r_s can be calculated according to relation (6) derived from Equation (5). The mentioned parameters were obtained from undisturbed soil samples taken into the rings with the volume of 100 cm^3 at the place of measuring the width of cracks.

$$r_s = \frac{log\left(\frac{V}{V_s}\right)}{log\left[\frac{-(\Delta z) + z_s}{z_s}\right]} \quad [–] \tag{6}$$

Theoretically, r_s can have the following values: $r_s = 1$ shrinkage cracks are not formed; the entire volume change is reflected in vertical movement; $1 < r_s < 3$ vertical movement predominates over formation of cracks; $r_s = 3$, isotropic shrinkage; $r_s > 3$, cracks formation predominates over vertical movement; $r_s \to \infty$, the entire volume change is reflected in the formation of cracks; there is no vertical movement.

From Equation (5), it is possible to derive relation (7) for calculating the volume change in the vertical plane

$$\Delta z = z_s - \left[\left(\frac{V}{V_s}\right)^{\frac{1}{r_s}}\right] z_s \qquad [\mathrm{L}] \tag{7}$$

Subsequently, according to Equation (8), it is possible to express volume V_h that are manifested in the horizontal plane, i.e. in changes in cracks volume.

$$V_h = V_s \left[\left(\frac{V}{V_s}\right)^{\frac{1}{r_s}} - \frac{V}{V_s}\right] \qquad [\mathrm{L}^3] \tag{8}$$

After measuring the volume of the soil samples in saturated state V_s and calculating the geometric factor r_s, the soil volume V is unknown in Equation (8) for the monitored volumetric soil moisture θ_v in the field. If $V = V_s - V_r$, then it is necessary to know the change in soil volume V_r [L^3] compared to saturated state V_s. During monitoring, each measured value of soil moisture corresponds to the soil volume change related to the value at saturated state. Therefore, it is useful to implement parameter d [%] which defines V_r size in % of V_s from Equation (5). Furthermore, the analytic expression of the empirical dependency $d = f(\theta_v)$, [%] is found. Second-degree polynomial function was identified as the most optimal expression of the sought relation. It can be expressed in the form:

$$d = a\,\theta_v^2 + b\,\theta_v + c \qquad [\%] \tag{9}$$

If the d is expressed as relative number to n, then it applies that $n = d/100$ $[-]$. $d \in \langle 0, c\rangle$ results from Equation (9), where c is Equation (9) parameter. If the F is the volume of saturated soil sample in % than it applies that $F = 100\%$. Subsequently, the volume of shrunken soil sample B can be expressed as $B = F - d$ or $B = F - n\,F$. If the volume changes in horizontal plane expressed in % of the F volume are designated as C than the Equation (8) is $C = F\left[(B/F)^{1/r_s} - B/F\right]$ [%]. If the m is proportional value of C, then $m = C / 100$ [–].

For thin soil layers (≤ 10 cm), subsequent calculations assume that the crack vertical dimensions are constant and tortuosity is neglected. On the investigated surface S_c of the two-domain soil structure (Fig. 6), the cracks length L_c [cm] in the crack network was measured.

The volume of the examined layer V_l on the investigated surface $S = x_l\,y_l$ of power z_l is

$$V_l = x_l\,y_l\,z_l \qquad [\mathrm{L}^3] \tag{10}$$

The volume of the cracks is

$$V_c = V_l\,m \qquad [\mathrm{L}^3] \tag{11}$$

The surface area of the cracks is

$$S_c = \frac{V_c}{z_l} = x_l\,y_l\,m \qquad [\mathrm{L}^2] \tag{12}$$

The average width of the cracks is

$$w_b = \frac{S_c}{L_c} \qquad [\mathrm{L}] \tag{13}$$

In the areas which are homogenous in soil texture, the length of cracks can be related to 1 m^2 and expressed as the specific length of cracks $L_{cm} = \frac{L_c}{S}$, [L L^{-2}]. In that case, the Equations 10 to 13 are adjusted to 1 m^2. Similarly, specific values for the volume V_{cm} and the surface area S_{cm} are obtained. From the total precipitation P, we can then easily calculate the total precipitation P_c (in mm) which fell per unit area through the surface area S_{cm} directly into the crack.

$$P_c = P\,S_{cm} \qquad [\mathrm{L}] \tag{14}$$

Calculated crack widths were compared with the measured values. The compliance of the calculated and measured values was assessed by a series of the statistical indicators (Nash and Sutcliffe, 1970):

root mean square error RMSE

$$RMSE = \sqrt{\frac{\sum_{i=1}^{n}(x_c - x_m)^2}{n}} \tag{15}$$

relative error index such as the Nash-Sutcliffe-Index (NS)

$$NS = \frac{\sum_{i=1}^{n}(x_c - x_m)^2}{\sum_{i=1}^{n}\left(x_m - x_{m_mean}\right)^2} \tag{16}$$

index of agreement (IA) (Willmott, 1982)

$$IA = 1 - \frac{\sum_{i=1}^{n}(x_c - x_m)^2}{\sum_{i-1}^{n}\left[\left|x_c - x_{m_mean}\right| + \left|x_m - x_{m_mean}\right|\right]^2} \tag{17}$$

where x_m are the measured values; x_{m_mean} are the average measured values; x_c are the calculated values of the examined indicators.

The NS index varies within the interval $NS \in (-\infty, 1\rangle$. NS values between 0 and 1 are considered an acceptable match between the measurement and calculation. If NS < 0 then the average measured value is a better predictor than the calculated value (Moriasi et al., 2007). IA values belong to the interval $IA \in \langle 0, 1\rangle$. Perfect agreement is considered when NS and IA indices approach 1. In addition, measured and calculated data were compared by the methods of descriptive statistics and statistical tests.

RESULTS AND DISCUSSION

Results of measurements and calculations

The source data of crack width measurements and their recalculation by Equation (2) are shown in Table 3. The parameters of the measuring tool are shown in Fig. 7. From the listed parameters, the value of the conversion constant $k = 0.652$ was calculated, so the rate of increase in crack width measurements is $en = 1.534$. On the examined surface area $S = 1.9$ m^2, the measured length of cracks was $L_c = 4.12$ m, which in specific length of cracks was $L_{cm} = 2.17$ m m^2.

Fig. 8 shows the course of the temperature measured in a crack in a depth of 0.1 m under the soil surface (T_c), the air temperature at soil surface (T_a), maximum (T_{d_max}) and minimum (T_{d_min}) daily air temperature 2 m above the soil surface. The temperature in the crack is higher than the minimum air temperatures 2 m above the soil surface. During sudden temperature drop due to precipitation event, the temperature in the crack is higher than the temperature at the soil surface.

Table 3. Results of crack width and air temperature measurements.

seq.	date	T_a	T_c	volumetric moisture [%]			avg	width at the top w_t [cm]			avg	width at the crack w_b [cm]			avg
		[°C]						1	2	3		1	2	3	
1	13.7.2022	22.7	18.7	26.20	25.80	24.90	**25.63**	5.80	5.00	4.50	**5.10**	3.78	3.26	2.94	**3.33**
2	14.7.2022	32.0	21.2	25.20	25.00	24.70	**24.97**	5.70	4.80	4.60	**5.03**	3.72	3.13	3.00	**3.28**
3	15.7.2022	26.1	23.6	24.50	24.40	24.70	**24.53**	5.00	4.70	4.73	**4.81**	3.26	3.07	3.09	**3.14**
4	18.7.2022	29.0	20.7	23.60	23.60	23.60	**23.60**	5.67	4.90	4.80	**5.12**	3.70	3.20	3.13	**3.34**
5	19.7.2022	25.7	22.4	23.50	23.50	23.40	**23.47**	5.20	4.85	4.80	**4.95**	3.39	3.16	3.13	**3.23**
6	25.7.2022	27.8	20.8	23.40	23.40	22.90	**23.23**	4.27	4.63	4.12	**4.34**	2.78	3.02	2.69	**2.83**
7	29.7.2022	27.0	24.0	21.50	21.40	21.40	**21.43**	4.20	4.10	4.10	**4.13**	2.74	2.67	2.67	**2.70**
8	1.8.2022	19.7	22.2	33.30	33.30	33.50	**33.37**	1.20	1.80	1.80	**1.60**	0.78	1.17	1.17	**1.04**
9	2.8.2022	28.0	22.8	27.20	27.40	27.50	**27.37**	1.20	1.60	1.60	**1.47**	0.78	1.04	1.04	**0.96**
10	3.8.2022	27.7	24.1	25.90	26.30	25.70	**25.97**	1.20	1.60	1.60	**1.47**	0.78	1.04	1.04	**0.96**
11	4.8.2022	26.7	20.7	25.00	25.00	24.70	**24.90**	1.20	1.70	1.70	**1.53**	0.78	1.11	1.11	**1.00**
12	9.8.2022	27.4	21.6	17.00	17.10	17.00	**17.03**	2.30	2.30	2.80	**2.47**	1.50	1.50	1.83	**1.61**
13	11.8.2022	24.0	20.8	13.90	13.90	14.00	**13.93**	2.30	2.20	2.90	**2.47**	1.50	1.43	1.89	**1.61**

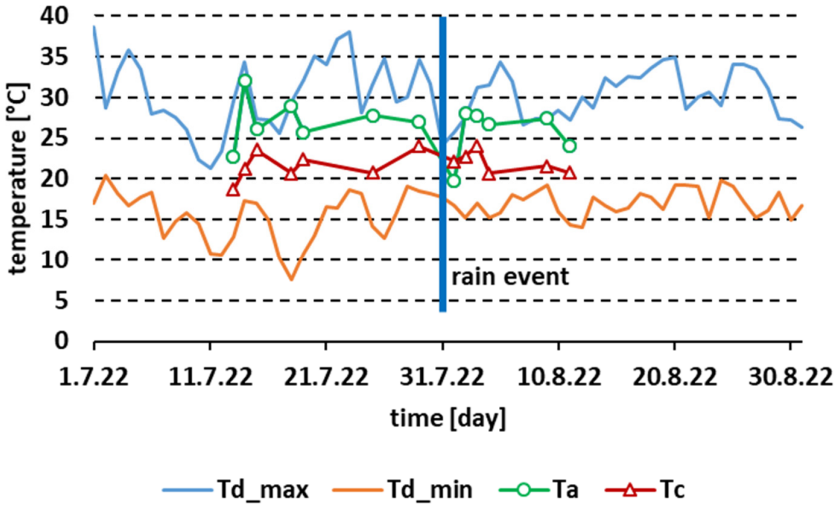


Fig. 8. The temperature curves during the investigated period.

The temperature curves indicate that water vapour can condense on the walls of the crack.

Table 4 shows the results of the measurements necessary for the calculation of the geometric factor r_s by Equation (6). The samples were taken in the investigated crack network (Fig. 6). The average value from two samples is 3.286 > 3.0, i.e. formation of cracks predominates over vertical movement.

Table 5 shows the measured values of the volume changes of the saturated soil sample during drying which were used to formulate the empirical relationship $d = f(\theta_v)$. The relationship is shown in Fig. 9. It is expressed by means of a second-degree polynomial function by Equation (9). The coefficients of the polynomial are $a = -0.0079$; $b = -0.0702$; $c = 17.778$. Correlation $R^2 = 0.98$ indicates that the measured values closely correlate with their analytical expressions.

Table 6 shows the results of the monitoring of volumetric soil moisture in the crack network and the measured and calculated values of crack widths. The table also shows the partial results of the crack width calculation. The measured and calculated surface length, width and surface area of the cracks on the soil surface are both calculated per unit area of 1 m^2. The unit thickness of the examined surface soil layer is 0.1 m. The measured values of average crack width range between $\langle 0.96, 3.34 \rangle$ [cm] and the calculated values range between $\langle 1.69, 3.82 \rangle$ [cm]. The calculated values show slightly less variation range. The calculated values of the crack width are overestimated. This is most evident in the set of low values. Therefore, the calculated results of cracks surface area on the soil surface as well as cracks volume in the examined layer are also affected. The surface area of cracks per unit of soil surface, determined by monitoring of cracks width, ranges between $\langle 0.0259, 0.0905 \rangle$ [m^2 m^{-2}]. Considering the examined soil environment, this represents surface changes of the cracks network between 2.59% and 9.05% of the investigated area. This means that 2.59% to 9.05% of precipitation or irrigation spray falls into the crack. The water in the crack penetrates deeper soil horizons until reaching the groundwater level. On the way, water interacts with the soil matrix. As a result, the moisture of the soil matrix increases and so does its volume. The increase in volume causes the decrease in geometric dimensions of the cracks.

On 30.7.2022, an important precipitation event occurred. During the event, precipitation total was 28.3 mm. The specific surface area of the cracks measured before the event (on 29.7.2022) was 0.0731 m^2 m^{-2} (Table 6). Equation (14) shows

Table 4. Measured parameters necessary for the calculation of the geometric factor r_s.

Layer	roller num.	z_s	V_s	V	z	Δz	r_s	avg (r_s)	Δz	V_r
[cm]		[cm]	[cm^3]	[cm^3]	[cm]	[cm]	[–]	[–]	[%]	[%]
0–10	1	3.33	99.48	82.25	3.14	0.20	3.15	3.29	5.85	17.31
	2	3.33	98.89	82.40	3.15	0.17	3.42		5.19	16.68

Table 5. Measured parameters used to formulate the relationship $d = f(\theta_v)$.

drying time	drying temperature	sample				d	mass moisture	θ_v
		weight	height	diameter	V			
[hours]	[°C]	[g]	[cm]	[cm]	[cm^3]	[%]	[%]	[%]
0	22	179.15	3.33	6.17	99.43	**0.00**	31.41	**43.04**
95	25	156.70	3.24	5.86	87.12	**12.38**	14.94	**23.37**
118	27.5	149.68	3.18	5.83	84.92	**14.59**	9.79	**15.71**
143	26	145.30	3.10	5.81	81.91	**17.62**	6.58	**10.95**
191	24	141.81	3.10	5.81	81.91	**17.62**	4.02	**6.69**
oven drying	105	136.33	3.10	5.81	81.91	**17.62**	0.00	**0.00**
0	22	177.74	3.33	6.15	98.84	**0.00**	32.17	**43.74**
81	26	158.70	3.15	5.99	88.58	**10.38**	18.01	**27.33**
95	25	153.15	3.15	5.99	88.58	**10.38**	13.88	**21.07**
118	27.5	146.90	3.15	5.81	83.37	**15.65**	9.24	**14.74**
143	26	143.24	3.15	5.81	83.37	**15.65**	6.51	**10.44**
191	24	139.95	3.13	5.78	81.99	**17.05**	4.07	**6.67**
oven drying	105	134.48	3.13	5.78	81.99	**17.05**	0.00	**0.00**

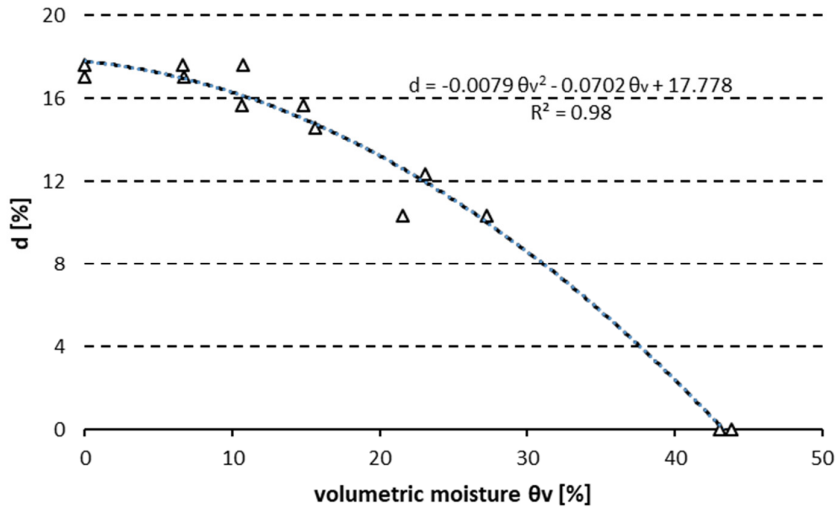


Fig. 9. Empirical relation between volume change d and volumetric moisture θ_v of the examined soil sample $d = f(\theta_v)$.

that the precipitation which fell directly into the crack was P_c = 2.07 mm i.e. 2.07 l m^{-2}. If the stated volume is related to a larger area, e.g. 1 ha, this precipitation event provides important water volume (20.7 m^3).

The presence of cracks in soil impacts potential infiltration surface through the walls of the cracks into the soil matrix during precipitation. Considering the specific length of cracks is 2.17 m m^2 and the layer thickness is 0.1 m, potential infiltration surface area of 0.434 m^2 m^{-2} is available. Assuming the soil profile is dried to a depth of 1 m (Fig. 4 and 5), infiltration surface area of 4.34 m^2 m^{-2} is available when cracks network is flooded during heavy rainfall. This is 4.34 times larger infiltration area than the infiltration area on the soil surface.

The retention volume of crack network is very important for rainfall-runoff relationships. On 29.7.2022, the measured specific retention volume of cracks (V_{cm}) was 7373 cm^3 m^{-2}. This volume represents a total precipitation of 73.1 mm. On ESL, the precipitation total with a periodicity of 0.01 is 76 mm. This is a considerable volume available for accepting sudden heavy rainfall. It should be noted here that water surface runoff in a two-domain soil environment occurs only after cracks are filled with water or after they have closed.

Cracks have a significant impact on transport processes, hydrodynamics of a soil profile and on rainfall-runoff processes in the areas with the potential for the formation of a two-domain soil structure.

Dynamics of cracks geometry dimensions on the surface

During the investigated period, on 30.7.2022 and 31.7.2022, a precipitation event occurred during which the precipitation total was 34.5 mm. The average crack width measured on 29.7.2022 was 2.7 cm. Volumetric soil moisture was below WP, 21.43%. The measurements after the precipitation event on 1.8.2022 showed that the volumetric soil moisture increased above TP, to 33.37%. The crack width narrowed by 1.7 cm to 1.0 cm. Under given soil and meteorological conditions, for the crack narrowing of 1 mm, 2 mm of precipitation is necessary. As a reaction to precipitation, soil volume changed rapidly. The entire narrowing of the crack occurred during two days of precipitation and did not change in the following days.

Fig. 10 is a graphical representation of the measured courses of volumetric soil moisture, precipitation and maximum and minimum daily temperatures. It also shows the monitored and calculated average crack widths and temporal development of the transverse dimensions of the cracks in the horizontal plane.

Fig. 10a illustrates the effects of changes in volumetric soil moisture on the cracks width. The lines show the dynamics of the interaction between soil moisture and soil volume changes in the horizontal plane. These interaction processes result in the changes in the geometric dimensions of the cracks, which are inversely proportional to the volumetric soil moisture. The course of the calculated and measured transverse dimensions of the cracks are also illustrated therein. The illustration clearly shows the differences between the calculated and measured widths of the cracks during wetting and drying of the soil.

Fig. 10b shows daily precipitation totals and the course of the maximum and minimum daily precipitation totals are shown for July and August. Time interval of the cracks network monitoring is also marked there. The figure shows the reaction of the soil profile to the precipitation event on 30.7.2022 and 31.7.2022. An increase in soil moisture and a decrease in crack porosity was identified.

This effect of precipitation is also evident in Fig. 10c. In both calculated and measured course, it is manifested by the narrowing of the crack width and its subsequent expansion during the following rainless days.

Model efficiency

The proposed calculation procedure was verified by Equations (15), (16) and (17). The series of values w_b and w_b^* from Table 6 were compared. The root mean square error expressed by the RMSE indicator was 1.21. The ideal values of NS and IA indices are close to 1. The optimal value of NS index is between 0 and 1. In our case, NS = –0.50, which is a negative value, but still close to 0. The value of IA = 0.50 is in the middle of the interval $\langle 0, 1 \rangle$.

Table 7 shows basic characteristics of the shape of a random variable distribution and variability. It indicates that the calculated and measured data are slightly different in their average values. There are significant differences in variability, both in absolute values and in relation to the average. The calculation does not record low values of the crack width. This is reflected in different variability of the calculated values and in the shape of their distribution curves. The statistical distribution of the calculated values is flatter compared to the normal distribution, while the distribution of the measured values is more skewed than the normal distribution. Both sets are skewed from the left, but the distribution of the measured values has a longer left end of the curve. In other words, the calculation model was not able to record lower values.

These findings were also confirmed by statistical tests *F*-test and *T*-test for comparison of variances and averages. The results of the *F*-test for comparing variances showed that there is a statistically significant difference between the standard deviation of two samples, at 95.0% reliability level. The null hypothesis of standard deviations equality can be rejected in favour of the hypothesis of their inequality. *T*-test for comparing two means showed that the *P*-value is not lower than 0.05 and the null hypothesis of equality of means cannot be rejected.

Table 6. Comparison of the calculated and measured average cracks width on the surface.

date	θ_v^*	d	B	C	V_{cm}	S_{cm}	S_{cm}^*	w_b	w_b^*
		Eq. (9)	$F - d$		Eq. (11)	Eq. (12)		Eq. (13)	
	[%]	[%]	[%]	[%]	[cm^3 m^{-2}]	[cm^2 m^{-2}]	[cm^2 m^{-2}]	[cm]	[cm]
13.7.2022	25.63	10.79	89.21	7.37	7373	737	901	2.7	3.3
14.7.2022	24.97	11.10	88.90	7.58	7583	758	890	2.8	3.3
15.7.2022	24.53	11.30	88.70	7.72	7717	772	850	2.8	3.1
18.7.2022	23.60	11.72	88.28	8.00	7998	800	905	3.0	3.3
19.7.2022	23.47	11.78	88.22	8.04	8038	804	875	3.0	3.2
25.7.2022	23.23	11.88	88.12	8.11	8106	811	767	3.0	2.8
29.7.2022	21.43	12.64	87.36	8.61	8614	861	731	3.2	2.7
1.8.2022	33.37	6.64	93.36	4.57	4571	457	283	1.7	1.0
2.8.2022	27.37	9.94	90.06	6.80	6804	680	259	2.5	1.0
3.8.2022	25.97	10.63	89.37	7.27	7267	727	259	2.7	1.0
4.8.2022	24.90	11.13	88.87	7.60	7604	760	271	2.8	1.0
9.8.2022	17.03	14.29	85.71	9.71	9706	971	436	3.6	1.6
11.8.2022	13.93	15.27	84.73	10.35	10350	1035	436	3.8	1.6

*the values measured in the field

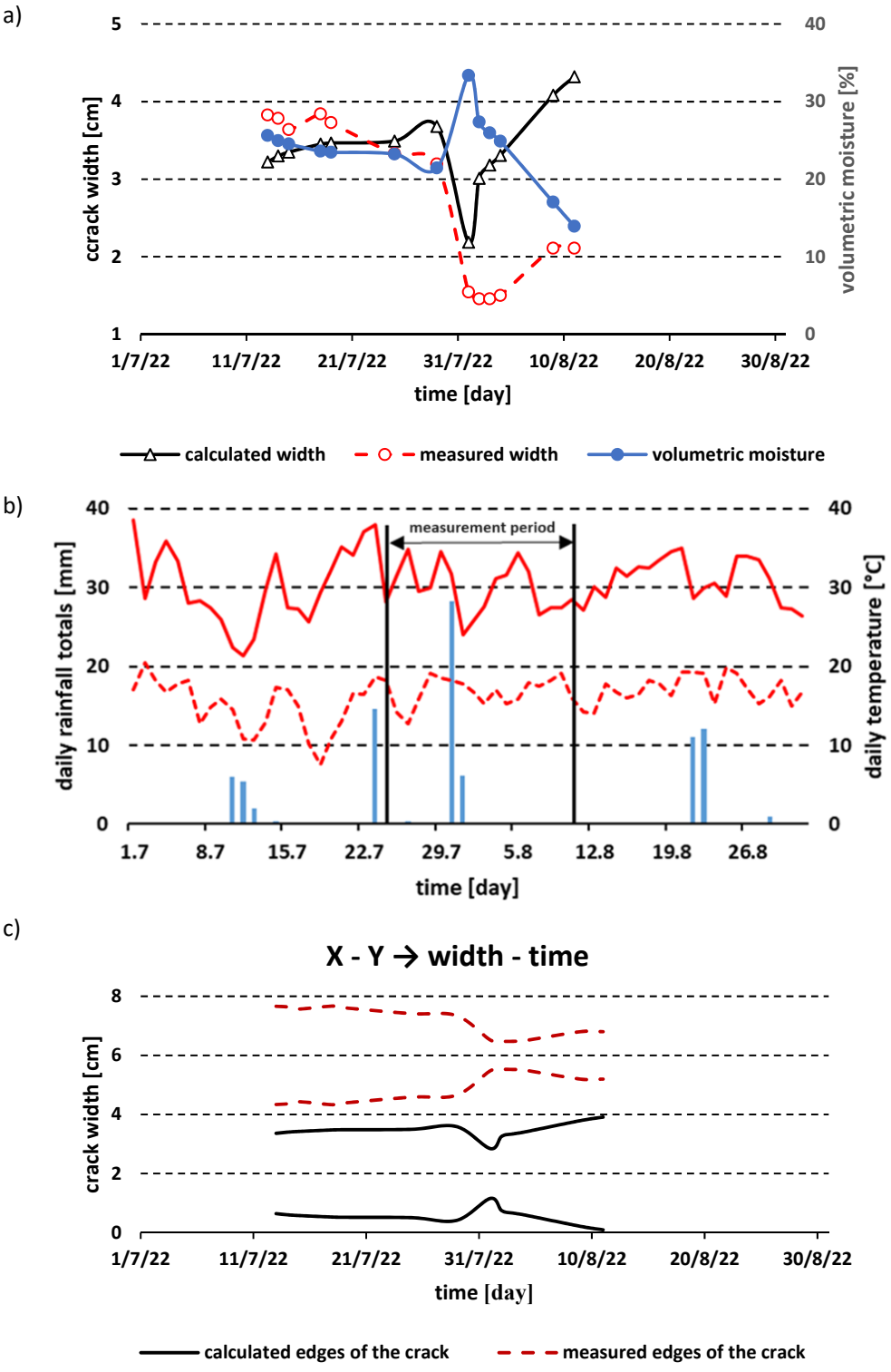


Fig. 10. Comparison of measured and calculated changes in crack width at the soil surface.

Two phases were recorded during the measurements. The first one from the beginning of the measurements until the precipitation event on 29.7.2022 and the second one from the precipitation event on 1.8.2022 until the end of the measurements. The first phase is rather balanced. The correlation expressed by the correlation coefficient is significant at logarithmic trend (R^2 = 0.62). During the precipitation event on 30.7.2022 and 31.7.2022, there was a significant reduction in the transverse dimensions of the cracks due to the swelling of the soil. The change expressed both by calculation and measurements is illustrated in Fig. 11. In the second phase, a significant upward trend in the expansion of cracks was recorded. The correlation is significant at logarithmic trend (R^2 = 0.64).

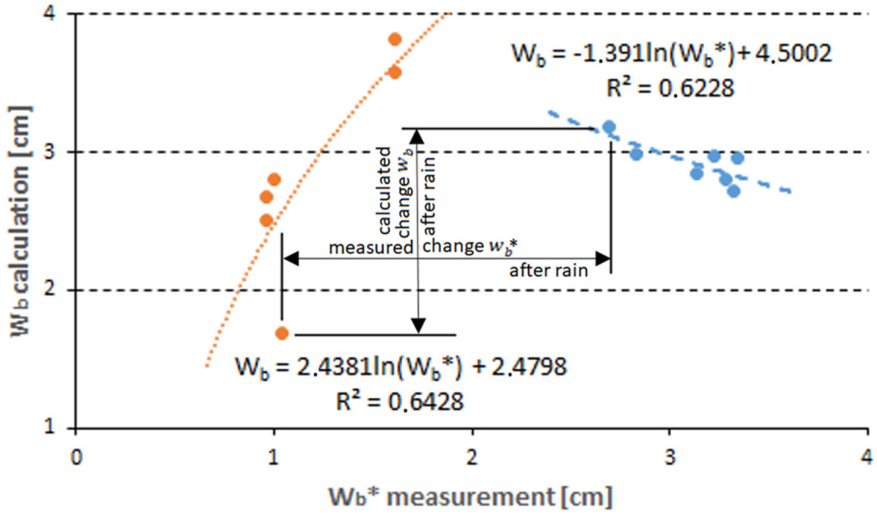


Fig. 11. Regression analysis and course of the measured w_b^* and calculated w_b cracks width before the precipitation event "●" and after the precipitation event "●".

Table 7. Descriptive statistics of the calculated and measured values of the crack width.

Statistical indicator	calculation	measurement
Mean	2.89	2.23
Standard Error	0.14	0.29
Median	2.85	2.70
Standard Deviation	0.51	1.04
Coefficient of variation C_v	0.18	0.46
Sample Variance	0.26	1.07
Kurtosis	2.36	–2.02
Skewness	–0.47	–0.20
Range	2.13	2.38
Minimum	1.69	0.96
Maximum	3.82	3.34
Sum	37.54	29.02
Count	13	13
Confidence level (95%)	0.31	0.63

The calculation procedure is suitable for basic estimation and assessment of changes in crack porosity in the vertical plane of a soil profile. It is sensitive to changes in soil moisture. It should be noted that for its wider use, it is required that shrinkage characteristics are determined in the vertical plane of a soil profile for different soil types, especially if the examined area is not homogeneous in terms of soil types. The disadvantage of the calculation method is that it does not record low values of the transverse dimensions of the cracks, which reduces the variability of the outputs compared to the measured values. Reasons for the inaccuracies of the calculated results with respect to the measurements can be different. The causes may be the aforementioned inhomogeneity of the soil environment, the effect of deeper soil horizons, inaccuracies in determining the shrinkage characteristics or simplifying assumptions (tortuosity, constant vertical crack dimensions). The existence and potential effect of hysteresis in the process of volume changes and water repellency (Doerr et al., 2003) may also be considered. In the model, cohesive and adhesive forces are not analysed. Cohesion and internal friction are strength parameters of soils (Gautam, 2018; Qiu et al., 2020). In summary, the model is evaluated as satisfactory for estimating the changes in crack width in the investigated soil layer.

CONCLUSION

Soil surface is a gateway for water to the unsaturated zone of a soil profile. Volume changes in heavy soils occurring during changes in soil moisture are caused by the high content of clay minerals. In the horizontal plane, these changes are manifested by the formation of a crack network on the soil surface. Crack network significantly changes the precipitation-runoff processes. Therefore, it is necessary to know the dynamics of crack network geometric dimensions.

The work presents the results of the measurements of the crack width in soil surface layer which is up to 0.1 m thick. A special device was designed for its accurate measurement. In order to determine the crack width, a calculation method based on the quantification of volume changes in relation to the volumetric soil moisture is proposed. The results of the calculations were verified by measurements in the field. The disadvantage of the calculation method is the fact that it neglects low values of the transverse dimensions of the cracks, what reduces the variability of the outputs compared to the measured values.

In the studied soil profile, formation of cracks predominates over vertical movement, geometric factor is $3.286 > 3$. The monitored average crack width ranged between $\langle 0.96, 3.34 \rangle$ [cm], the calculated widths ranged between $\langle 1.69, 3.82 \rangle$ [cm]. The surface area of cracks on the unit soil surface determined from the measurement of their width ranged between $\langle 0.0259, 0.0905 \rangle$ [m^2 m^{-2}]. In the examined soil environment, this represents surface changes of the crack network between 2.59% and 9.05% of the studied area. Under field conditions, this means that from 2.59% to 9.05% of precipitation or irrigation spray falls directly into the crack. During the crack network monitoring and at the time of extreme drought, one significant precipitation event occurred. During this event, on 30.7.2022 and 31.7.2022, the precipitation total was 34.5 mm. Direct precipitation which fell into the crack was P_c = 2.07 mm i.e. 2.07 l m^{-2}. Assuming that the soil profile was evenly dried up to 1 m, the retention volume of cracks per unit area of 1 m^2 was estimated to 73.1 mm. In the examined area, this precipitation event approaches precipitation with a periodicity of 0.01 (76 mm).

In the areas with the occurrence of heavy soils, it is necessary to deepen knowledge about their water regime for the forecast of the hydrological processes in this natural environment.

Acknowledgements. Authors are grateful to Scientific Grant Agency of the Ministry of Education, Science, Research and Sport of the Slovak Republic: (project VEGA No. 2/0044/20).

REFERENCES

Almikaeel, W., Čubanová, L., Šoltész, A., 2022. Hydrological drought forecasting using machine learning – Gidra river case study. Water, 14, 3, 387. DOI: 10.3390/w14030387

Amorim, C.L.G., Lopes, R.T., Barroso, R.C., Queiroz, J.C., Alves, D.B., Perez, C.A., Schelin, H.R., 2007. Effect of clay–water interactions on clay swelling by X-ray diffraction. Nuclear Instruments and Methods in Physics Research Section A: Accelerators, Spectrometers, Detectors and Associated Equipment, 580, 1, 768–770.

Baroková, D., Červeňanská, M., Šoltész, A., 2020. Assessment of the impact of proposed cut-off walls on ground-water level regime during extreme hydrological conditions. Acta Hydrologica Slovaca, 21, 1, 113–122.

Benetin, J., Šoltész, A., Štekauerová, V., 1985. Bilančný matematický model na podrobnú analýzu časovej variability zložiek vodného režimu pôd. Journal of Hydrology and Hydromechanics, 33, 585–609. (In Slovak.)

Beven, K., Germann, P.F., 1982. Macropores and water flow in soils. Wat. Resour. Res., 18, 5, 1311–1325.

Bronswijk, J.J.B., Evers-Vermeer, J.J., 1990. Shrinkage of Dutch clay soil aggregates. Netherlands Journal of Agricultural Science, 38, 175–194.

Bronswijk, J.J.B., 1988. Modeling of water balance, cracking and subsidence of clay soils. J. Hydrol., 97, 199–212.

Bronswijk, J.J.B., 1990. Shrinkage geometry of a heavy clay soil at various stresses. Soil Sci. Soc. Am. J., 54, 1500–1502.

Chen, W.L., Grabowski, R.C., Goel, S., 2022. Clay Swelling: Role of Cations in Stabilizing/ Destabilizing Mechanisms. ACS Omega. 2022 Jan 17; 7, 4, 3185–3191. DOI: 10.1021/acsomega.1c04384. PMID: 35128231; PMCID: PMC8811774.

Chertkov, V.Y., Ravina, I., 1999. Crack tortuosity in swelling clay soils. Int. Agrophysics, 13, 7–13.

Chertkov, V.Y., 2001. The horizontal hydraulic conductivity of interaggregate capillary cracks in clay soils. New letter EGS, Nice, 2001, 123 p.

Chertkov, V.Y., 2002. Modelling cracking stages of saturated soils as they dry and shrink. European Journal of Soil Science, 53, 1, 105–118.

Chertkov, V.Y., Ravina, I., 2011. Effect of interaggregate capillary cracks on the hydraulic conductivity of swelling clay soils. Water Resources Research, 37, 5, 1245–1256.

Cools, N., De Vos, B., 2010. 6th FSCC Interlaboratory Comparison 2009. Rapporten van het Instituut voor Natuur- en Bosonderzoek 2010 (rapportnr. 4). Instituut voor Natuur- en Bosonderzoek, Brussel. Report_Soil_Physical_RT_060510 (inbo.be).

Crescimanno, G., Iovino, M., Provenzano, G., 1995. Influence of salinity and sodicity on soil structural and hydraulic characteristics. Soil Sci. Soc. Am. J., 59, 1701–1708.

Čubanová, L., Šoltész, A., Mydla, J., 2022. Analysis of droughts due to the operation of water structures: Gidra river case study. Pollack Periodica, 17, 1, 111–116. DOI: 10.1556/606.2021.00463

Čurlík, J., Bedrna, Z., 1971. Príspevok k mineralogicko-morfologickému štúdiu illimerizovaných pôd na Východoslovenskej nížine. Vedecké práce VÚPVR, Bratislava, 5. (In Slovak.)

Dane, J.H., Hopmans, J.W., 2002. Pressure plate extractor. In: Dane, J.H., Topp, G.C. (Eds.): Methods of Soil Analysis: Physical Methods, Part 4. Soil Science Society of America, Madison, pp. 688–690.

Doerr, S.H., Ferreira, A.J.D., Walsh, R.P.D., Shakesby, R.A., Leighton-Boyce, G., Coelho, C.O.A., 2003. Soil water repellency as a potential parameter in rainfall-runoff modelling: experimental evidence at point to catchment scales from Portugal. Hydrological Processes, 17, 2, 363–377.

Doležal, F., 2001. Remarks to the physics of water movement and solute transport in swelling soils with cracks. In: Proc. Joint Meeting of the CSSS and SSSA, Prague, pp. 265–274.

Đukić, V., Erić, R., Dumbrovsky, M., Sobotkova, V., 2021. Spatio-temporal analysis of remotely sensed and hydrological model soil moisture in the small Jičinka River catchment in Czech Republic. Journal of Hydrology and Hydromechanics, 69, 1, 1–12. https://doi.org/10.2478/johh-2020-0038

Gautam, T.P., 2018. Cohesive soils. In: Bobrowsky, P.T., Marker, B. (Eds): Encyclopedia of Engineering Geology. Encyclopedia of Earth Sciences Series. Springer, Cham. https://doi.org/10.1007/978-3-319-73568-9_60

Gerke, H.H., van Genuchten, M.Th., 1993. A dual porosity model for simulating the prefevential movemoment of water and solutes in structed media. Water Resources Research, 29, 2, 305–319.

Hallett, P.D., Dexter, A.R., Yoshida, S., 2013. A history of understanding crack propagation and the tensile strength of soil. In: Logsdon, S., Berli, M., Horn, R. (Eds.): Quantifying and Modeling Soil Structure Dynamics. Soil Science Society of America. https://doi.org/10.2134/advagricsystmodel3.c5

Hansen, E.L., Hemmen, H., Fonseca, D.D.M., Coutant, C., Knudsen, K.D., Plivelic, T.S., Bonn, D., Fossum, J.O., 2012. Swelling transition of a clay induced by heating. Scientific Reports, 2, 618, 1–4. https://doi.org/10.1038/srep00618

ISO 11274, 1998. Soil Quality - Determination of The Water-Retention Characteristic - Laboratory Methods. International Organization for Standardization, Geneva, Switzerland, 20 p. (webstore.ansi.org/standards/iso/iso112741998).

Jarvis, N.J., 1994. The MACRO Model (Version 3.1) – Technical Description and Sample Simulations. Monograph – Department of Soil Sciences, Swedish University of Agricultural Sciences, Uppsala, 52 p.

Johnston, C.T., 2018. 4–Clay mineral–water interactions. In: Schoonheydt, R., Johnston, C.T., Bergaya, F. (Eds.): Developments in Clay Science, Vol. 9, Elsevier, pp. 89–124. https://doi.org/10.1016/B978-0-08-102432-4.00004-4

Krisnanto, S., Rahardjo, H., Fredlund, D.G., Leong, E.C., 2016. Water content of soil matrix during lateral water flow through cracked soil. Engineering Geology, 210, 168–179. https://doi.org/10.1016/j.enggeo.2016.06.012

Kuban, M., Parajka, J., Tong, R., Greimeister-Pfeil, I., Vreugdenhil, M., Szolgay, J., Kohnova, S., Hlavcova, K., Sleziak, P., Brziak, A., 2022. The effects of satellite soil moisture data on the parametrization of topsoil and root zone soil moisture in a conceptual hydrological model. Journal of Hydrology and Hydromechanics, 70, 3, 295–307. https://doi.org/10.2478/johh-2022-0021

Moriasi, D.N., Arnold, J.G., Van Liew, M.W., Bingner, R.L., Harmel, R.D., Veith, T.L., 2007. Model evaluation guidelines for systematic quantification of accuracy in watershed simulations. Trans. ASABE, 50, 885–900. https://doi.org/10.13031/2013.23153

Nash, J.E., Sutcliffe, J.V., 1970. River flow forecasting through conceptual models. Part 1: a discussion of principles. Journal of Hydrology, 10, 282–290.

Novák, V., Šoltész, A., 1994. Infiltration of water into cracked soil.

Water and solute. In: Proceedings Wageningen Symposium – Water and solute movement in heavy clay soils for land reclamation and improvement. ILRI, Wageningen, pp. 148–151.

Novák, V., 1978. Vplyv pôdnych puklín na vodný režim ťažkých pôd. Journal of Hydrology and Hydromechanics, 26, 4, 487–492. ISSN 0042-790X. (In Slovak.)

Novák, V., 2000. Charakteristiky pôdy s puklinami: Merná dĺžka puklín na povrchu pôdy. Acta Hydrologica Slovaca, 1, 2, 175–181. (In Slovak.)

Qiu, T., Liu, C., Zhong, X., Zhu, Y., 2020. Experimental research on the impact of temperature on the adhesion characteristics of soil-structure interface. Geofluids, 2020, Article ID 6675576, 9 p. https://doi.org/10.1155/2020/6675576

Richards, L.A., 1931. Capillary conduction of liquids through porous mediums. Physics, 1, 318–333.

Ross, G.J., 1978. Relationships of specific surface area and clay content to shrink – swell potential of soils having different clay mineralogical composition. Canadian Journal Soil Science. 58, 159–166.

Ross, P.J., 1990. Efficient numeral method for infiltration using Richards equation. Water Resources Research, 26, 2, 819–829.

Šimůnek, J., van Genuchten, M.T., Jacques, D., Šejna, M., 2017. Recent developments and applications of the HYDRUS software packages. In: Abstracts of the 5th International Conference HYDRUS Software Applications to Subsurface Flow and Contaminant Transport Problems, Prague, p. 41.

Stewart, R.D., Najm, M.R.A., 2020. Field measurements of soil cracks. Soil Sci. Soc. Am. J., 84, 1462–1476. https://doi.org/10.1002/saj2.20155

Tang, C.-S., Cui, Y.-J., Tang, A.-M., Shi, B., 2010. Experiment evidence on the temperature dependence of desiccation cracking behavior of clayey soils. Engineering Geology, 114, 261–266.

Tang, C-S., Zhu, C., Cheng, Q., Zeng, H., Xu, J-J., Tian, B-G., Shi, B., 2021. Desiccation cracking of soils: A review of investigation approaches, underlying mechanisms, and influencing factors. Earth-Science Reviews, 216, 103586. https://doi.org/10.1016/j.earscirev.2021.103586

Tang, Y., Yang, B., Zhao, X., Yang, C., 2023. Structural and fractal analysis of soil cracks due to the roots of *Setaria Viridis*. Fractal Fract., 7, 19. https://doi.org/10.3390/fractalfract7010019

van Genuchten, M.Th., Schaap, M.G., Mohanty, B.P., Šimůnek, J., Leij, F.J., 2000. Modelling flow and transport proceses at the local scale. Modelling of transport processes in soils at various scales in time and space. In: International Workshop of Eur. Ag. Engs. Field of Interest on Soil a Water, Leuwen, Belgium, pp. 23–45.

Velde, B., 1995. Composition and mineralogy of clay minerals. In: Velde, B. (Ed.): Origin and Mineralogy of Clays. Springer, New York, pp. 8–42.

Willmott, C.J., 1982. Some comments on the evaluation of model performance. Bull. Am. Meteorol. Soc., 63, 1309–1313. https://doi.org/10.1175/1520-0477(1982)063<1309:SCOTEO>2.0.CO;2.

Zurmuhl, T., Durner, W., 1996. Modelling transient water and solute transport in a biporous soil. Water Resources Research, 32, 819–829.

Received 27 February 2023
Accepted 16 October 2023